Associated $t\bar{t}H$ production at the LHC: Theoretical predictions at NLO + NNLL accuracy

Anna Kulesza,[1,*] Leszek Motyka,[2,†] Tomasz Stebel,[2,3,‡] and Vincent Theeuwes[4,§]

[1]*Institute for Theoretical Physics, WWU Münster, D-48149 Münster, Germany*
[2]*Institute of Physics, Jagiellonian University, S.Łojasiewicza 11, 30-348 Kraków, Poland*
[3]*Institute of Nuclear Physics PAN, Radzikowskiego 152, 31-342 Kraków, Poland*
[4]*Department of Physics, SUNY Buffalo, 261 Fronczak Hall, Buffalo, New York 14260-1500, USA*

(Received 19 October 2017; revised manuscript received 5 April 2018; published 8 June 2018)

We perform threshold resummation of soft gluon corrections to the total cross section and the invariant mass distribution for the process $pp \to t\bar{t}H$. The resummation is carried out at next-to-next-to-leading-logarithmic (NNLL) accuracy using the direct QCD Mellin space technique in the three-particle invariant mass kinematics. After presenting analytical expressions we discuss the impact of resummation on the numerical predictions for the associated Higgs boson production with top quarks at the LHC. We find that next-to-leading-order (NLO)+NNLL resummation leads to predictions for which the central values are remarkably stable with respect to scale variation and for which theoretical uncertainties are reduced in comparison to NLO predictions.

DOI: 10.1103/PhysRevD.97.114007

I. INTRODUCTION

The measurement of Higgs boson production rates in the $pp \to t\bar{t}H$ process is of central importance to the LHC research program. The process has been intensively searched for in run 1 [1–5], and its measurement is among the highest priorities of the LHC run 2 physics program [6–8]. The associated production process offers a direct way to probe the strength of the top–Higgs Yukawa coupling without making any assumptions regarding its nature. As the top–Higgs Yukawa coupling is especially sensitive to the underlying physics, $t\bar{t}H$ production provides a vital test of the Standard Model (SM) and possibly a means to probe the beyond the SM physics indirectly. It is thus highly important that precise and reliable theoretical predictions are available for this process.

For these reasons, a large amount of effort has been invested to improve the theoretical description of the $t\bar{t}H$ production. The next-to-leading-order (NLO) QCD, i.e. $\mathcal{O}(\alpha_s^3\alpha)$, predictions were obtained some time ago [9,10]. They have been newly recalculated and matched to parton showers in [11–14]. In the last years, the mixed QCD-weak corrections [15] and QCD-EW corrections [16,17] of $\mathcal{O}(\alpha_s^2\alpha^2)$ are also available. Furthermore, the NLO electroweak (EW) and QCD corrections to the hadronic $t\bar{t}H$ production with off shell top and antitop quarks have been recently obtained [18,19]. For the most part, the NLO QCD corrections are ∼20% at the run 2 LHC energies, whereas the size of the (electro)weak correction is more than 10 times smaller. The scale uncertainty of the NLO QCD corrections is estimated to be ∼10% [9,10,20].

In general, if for a given process one expects that a significant part of higher order corrections originates from the emission of soft and/or collinear gluons, it is possible to improve the accuracy of theoretical predictions by employing methods of resummation. Relying on principles of factorization between various dynamical modes, they allow an all-order calculation of dominant logarithmic corrections originating from a certain kinematical limit. Supplementing fixed-order results with resummation leads not only to a change in the value of the cross section but also offers a better control over the theoretical error, in particular due to cancellations of the factorization scale dependence between parton distribution functions (pdfs) and the partonic cross sections. The universality of resummation concepts warrants their applications to scattering processes with arbitrary many partons in the final state [21,22], thus also to class $2 \to 3$ processes and in particular the associated $t\bar{t}H$ production at the LHC.

The first step in this direction was performed by us in [23], where we presented the first calculation of the resummed total cross section for the $t\bar{t}H$ production at the next-to-leading-logarithmic (NLL) accuracy. The calculation relied

*anna.kulesza@uni-muenster.de
†leszekm@th.if.uj.edu.pl
‡tomasz.stebel@uj.edu.pl
§vincent.theeuwes@uni-goettingen.de

on application of the traditional Mellin-space resummation formalism in the absolute threshold limit, i.e., in the limit of the partonic energy $\sqrt{\hat{s}}$ approaching the production threshold $M = 2m_t + m_H$, $\hat{s} \to M^2$, where m_t is the top quark mass and m_H is the Higgs boson mass. In [23], we have achieved an all-order improvement of the theoretical predictions by taking into account a well-defined subclass of higher order corrections. However, due to the suppression of the available 3-particle phase-space in the absolute production threshold limit, it is to be expected that the numerical impact of formally large logarithmic corrections resummed in these kinematics will be somewhat diminished and that contributions prevailing numerically might come from regions further away from the absolute threshold scale M.

Subsequently we have performed [24] resummation of NLL corrections arising in the limit of $\sqrt{\hat{s}}$ approaching the invariant mass threshold Q with $Q^2 = (p_t + p_{\bar{t}} + p_H)^2$. We have considered cross sections differential in the invariant mass Q, as well as the total cross sections obtained after integration over Q. For a $2 \to 2$ process, this type of resummation is often referred to as threshold resummation in the pair-invariant mass (PIM) kinematics. Threshold resummation can be also performed in the framework of the soft-collinear effective theory (SCET). The first application of this technique to a $2 \to 3$ process, more specifically to the process $pp \to t\bar{t}W^{\pm}$, was presented in [25]. The SCET framework was also used to obtain an approximation of the next-to-next-to-leading order (NNLO) $t\bar{t}H$ cross section and distributions [26], following from the expansion of the NNLL resummation formula. Recently, NNLL results for $t\bar{t}W$ [27], $t\bar{t}H$ [28] and $t\bar{t}Z$ [29] associated production processes appeared, based on expressing the SCET formulas in Mellin space.

In this paper, we continue the work presented in [24] and perform threshold resummation in the invariant mass limit at the NNLL accuracy using the direct QCD [30] Mellin-space approach. Compared to NLL calculations, the anomalous dimensions governing resummation need to be implemented with an accuracy higher by 1 order. In contrast to the absolute threshold limit considered in [23], the soft anomalous dimension is a matrix in the color space containing nonzero off diagonal elements, thus requiring an implementation of the diagonalization procedure. We then match our NNLL cross section with the fixed-order cross section at NLO. The invariant mass kinematics also offers an opportunity to perform resummation for the differential distributions in Q.

The paper is structured as follows. In Sec. II we review threshold resummation in Mellin space, stressing the difference between the resummation in the invariant mass and the absolute threshold limits. The numerical results and their discussion is presented in Sec. III, where we also compare our results to those in [28]. We summarize our most important findings in Sec. IV.

II. NNLL RESUMMATION IN THE TRIPLE INVARIANT MASS KINEMATICS FOR $2 \to 3$ PROCESSES WITH TWO MASSIVE COLORED PARTICLES IN THE FINAL STATE

The resummation of soft gluon corrections to the differential cross section $d\sigma_{pp\to t\bar{t}H}/dQ^2$ is performed in Mellin space, where the Mellin moments are taken with respect to the variable $\rho = Q^2/S$. At the partonic level, the Mellin moments for the process $ij \to klB$, where i, j denote massless colored partons, k, l two massive quarks and B a massive color-singlet particle, are given by

$$\frac{d\tilde{\hat{\sigma}}_{ij\to klB}}{dQ^2}(N, Q^2, \{m^2\}, \mu_F^2, \mu_R^2) = \int_0^1 d\hat{\rho}\hat{\rho}^{N-1}\frac{d\hat{\sigma}_{ij\to klB}}{dQ^2}(\hat{\rho}, Q^2, \{m^2\}, \mu_F^2, \mu_R^2), \quad (1)$$

with $\hat{\rho} = Q^2/\hat{s}$ and $\{m^2\}$ denoting all masses entering the calculations.

Taking the Mellin transform allows one to systematically treat the logarithmic terms of the form $\alpha_s^n[\log^m(1-z)/(1-z)]_+$, with $m \le 2n-1$ and $z = Q^2/\hat{s}$, appearing in the perturbative expansion of the partonic cross section to all orders in α_s. In Mellin space these logarithms turn into logarithms of the variable N, and the threshold limit $z \to 1$ corresponds to the limit $N \to \infty$.

The resummed cross section in the N-space has the form [31,32][1]

$$\begin{aligned}\frac{d\tilde{\hat{\sigma}}^{(\mathrm{res})}_{ij\to klB}}{dQ^2}(N, Q^2, \{m^2\}, \mu_F^2, \mu_R^2) &= \mathrm{Tr}[\mathbf{H}_{ij\to klB}(Q^2, \{m^2\}, \mu_F^2, \mu_R^2) \\ &\times \mathbf{S}_{ij\to klB}(N+1, Q^2, \{m^2\}, \mu_R^2)] \\ &\times \Delta^i(N+1, Q^2, \mu_F^2, \mu_R^2)\Delta^j(N+1, Q^2, \mu_F^2, \mu_R^2), \quad (2)\end{aligned}$$

where the trace is taken over color space. The appearance of color dependence in Eq. (2) is inherently related to the fact that soft radiation is coherently sensitive to the color structure of the hard process from which it is emitted. The matrix $\mathbf{H}_{ij\to klB}$ indicates the hard-scattering contributions, absorbing the off shell effects, projected onto the chosen color basis. The color matrix $\mathbf{S}_{ij\to klB}$ represents the soft wide-angle emission. The functions Δ^i and Δ^j sum the logarithmic contributions due to (soft-)collinear radiation from the incoming partons. The radiative factors are thus universal for a specific initial state parton; i.e., they

[1]In fact, the soft function $\mathbf{S}_{ij\to klB}$ as well as the radiative factors Δ^i, Δ^j are dimensionless functions of the ratios of the scales and the coupling constant at the renormalization scale. The current notation indicating dependence on the scales is introduced for brevity.

depend neither on the underlying color structure nor the process.

At LO the $t\bar{t}H$ production receives contributions from the $q\bar{q}$ and gg channels. We analyze the color structure of the underlying processes in the s-channel color bases, $\{c_I^q\}$ and $\{c_I^g\}$, with

$$c_{\mathbf{1}}^q = \delta^{\alpha_i\alpha_j}\delta^{\alpha_k\alpha_l}, \qquad c_{\mathbf{8}}^q = T^a_{\alpha_i\alpha_j}T^a_{\alpha_k\alpha_l},$$
$$c_{\mathbf{1}}^g = \delta^{a_ia_j}\delta^{\alpha_k\alpha_l}, \qquad c_{\mathbf{8S}}^g = T^b_{\alpha_l\alpha_k}d^{ba_ia_j}, \qquad c_{\mathbf{8A}}^g = iT^b_{\alpha_l\alpha_k}f^{ba_ia_j}.$$

The hard function $\mathbf{H}_{ij\to klB}$ carries no dependence on N and is given by the perturbative expansion

$$\mathbf{H}_{ij\to klB} = \mathbf{H}^{(0)}_{ij\to klB} + \frac{\alpha_s}{\pi}\mathbf{H}^{(1)}_{ij\to klB} + \ldots \tag{3}$$

In order to perform resummation at NLL accuracy one needs to know $\mathbf{H}^{(0)}_{ij\to klB}$, whereas NNLL accuracy requires the knowledge of the $\mathbf{H}^{(1)}_{ij\to klB}$ coefficient.

The soft function, on the other hand, resums logarithms of N at the rate of one power of the logarithm per power of the strong coupling. These single logarithms due to the soft emission can be confronted with double logarithms due to soft and collinear emissions resummed by the jet factors Δ^i and Δ^j. As a dimensionless function, $\mathbf{S}_{ij\to klB}$ depends only on the ratio of the scales. At the same time, the dependence on N enters only via Q/N [33], making $\mathbf{S}_{ij\to klB}$ dependent on the ratio $Q/(N\mu_R)$. The soft function is given by a solution of the renormalization group equation [31,34] and has the form

$$\begin{aligned}\mathbf{S}_{ij\to klB}(N,Q^2,\{m^2\},\mu_R^2) &= \bar{\mathbf{U}}_{ij\to klB}(N,Q^2,\{m^2\},\mu_R^2)\tilde{\mathbf{S}}_{ij\to klB}(\alpha_s(Q^2/\bar{N}^2)) \\ &\times \mathbf{U}_{ij\to klB}(N,Q^2,\{m^2\},\mu_R^2),\end{aligned} \tag{4}$$

where $\tilde{\mathbf{S}}_{ij\to klB}$ plays a role of a boundary condition and is obtained by taking $\mathbf{S}_{ij\to klB}$ at $Q^2/(\bar{N}^2\mu_R^2) = 1$ with $\bar{N} = Ne^{\gamma_E}$ and γ_E denoting the Euler constant. It is a purely eikonal function [31,34,35] and can be calculated perturbatively

$$\tilde{\mathbf{S}}_{ij\to klB} = \tilde{\mathbf{S}}^{(0)}_{ij\to klB} + \frac{\alpha_s}{\pi}\tilde{\mathbf{S}}^{(1)}_{ij\to klB} + \ldots \tag{5}$$

At the lowest order the color matrix is given by

$$(\tilde{\mathbf{S}}^{(0)}_{ij\to kl})_{IJ} = \mathrm{Tr}[c_I^\dagger c_J]. \tag{6}$$

Similarly to the hard function, knowledge of $\mathbf{S}^{(0)}_{ij\to klB}$ is required in order to perform resummation at NLL accuracy and a result for $\mathbf{S}^{(1)}_{ij\to klB}$ at the NNLL accuracy. The scale of α_s in $\tilde{\mathbf{S}}_{ij\to kl}$, equal to $Q^2/\bar{N}^2$, results in an order $\alpha_s^2\log\bar{N}$ term if we expand $\tilde{\mathbf{S}}_{ij\to kl}$ in $\alpha_s(\mu_R^2)$.

The soft function evolution matrices $\bar{\mathbf{U}}_{ij\to klB}$, $\mathbf{U}_{ij\to klB}$ contain logarithmic enhancements due to soft wide-angle emissions [31,36][2]

$$\begin{aligned}&\bar{\mathbf{U}}_{ij\to klB}(N,Q^2,\{m^2\},\mu_R^2) \\ &\quad = \bar{\mathrm{P}}\exp\left[\int_{\mu_R}^{Q/\bar{N}}\frac{dq}{q}\mathbf{\Gamma}^\dagger_{ij\to klB}(\alpha_s(q^2))\right], \\ &\mathbf{U}_{ij\to klB}(N,Q^2,\{m^2\},\mu_R^2) \\ &\quad = \mathrm{P}\exp\left[\int_{\mu_R}^{Q/\bar{N}}\frac{dq}{q}\mathbf{\Gamma}_{ij\to klB}(\alpha_s(q^2))\right],\end{aligned} \tag{7}$$

where P and $\bar{\mathrm{P}}$ denote the path- and reverse path-ordering in the variable q, respectively. The soft anomalous dimension $\mathbf{\Gamma}_{ij\to klB}$ is a perturbative function in α_s,

$$\mathbf{\Gamma}_{ij\to klB}(\alpha_s) = \left[\left(\frac{\alpha_s}{\pi}\right)\mathbf{\Gamma}^{(1)}_{ij\to klB} + \left(\frac{\alpha_s}{\pi}\right)^2\mathbf{\Gamma}^{(2)}_{ij\to klB} + \ldots\right]. \tag{8}$$

In order to perform resummation at NLL accuracy we need to know $\mathbf{\Gamma}^{(1)}_{ij\to klB}$, whereas NNLL accuracy requires including $\mathbf{\Gamma}^{(2)}_{ij\to klB}$. The one-loop soft anomalous dimension for the process $ij\to klB$ with k, l being heavy quarks can be found e.g., in [23]. The two-loop contributions to the soft anomalous dimension were calculated in [37,38][3] In the triple-invariant mass (TIM) kinematics, the soft anomalous dimension matrix in general contains off diagonal terms, thus complicating the evaluation of the resummed cross section. At NNLL additional difficulty arises because of noncommutativity of $\mathbf{\Gamma}^{(1)}_{ij\to klB}$ and $\mathbf{\Gamma}^{(2)}_{ij\to klB}$ matrices.

We make use of the method of [31] in order to diagonalize the one-loop soft anomalous dimension matrix. Denoting the diagonalization matrix for $\mathbf{\Gamma}^{(1)}_{ij\to klB}$ by $\mathbf{R}$ we have

$$\mathbf{\Gamma}^{(1)}_R = \mathbf{R}^{-1}\mathbf{\Gamma}^{(1)}_{ij\to klB}\mathbf{R}, \tag{9}$$

where the diagonalized matrix is given by eigenvalues $\lambda_I^{(1)}$ of $\mathbf{\Gamma}^{(1)}_{ij\to klB}$

$$\mathbf{\Gamma}^{(1)}_{R,IJ} = \lambda_I^{(1)}\delta_{IJ},$$

and can be also written as $\mathbf{\Gamma}^{(1)}_R = [\vec{\lambda}^{(1)}]_D$ with $\vec{\lambda}^{(1)} = \{\lambda_1^{(1)},\ldots,\lambda_D^{(1)}\}$. The other matrices are transformed as

[2]For simplicity, the argument dependence of the soft anomalous dimension on the mass scales is suppressed in Eq. (7).

[3]Note that while using the radiative factors as given in [39,40], we need to subtract the collinear soft radiation already included in Δ^i, Δ^j from the eikonal cross section used to calculate the soft function.

$$\begin{aligned}\mathbf{\Gamma}_R^{(2)} &= \mathbf{R}^{-1}\mathbf{\Gamma}^{(2)}_{ij\to klB}\mathbf{R},\\ \mathbf{H}_R &= \mathbf{R}^{-1}\mathbf{H}_{ij\to klB}(\mathbf{R}^{-1})^\dagger,\\ \tilde{\mathbf{S}}_R &= \mathbf{R}^\dagger\tilde{\mathbf{S}}_{ij\to klB}\mathbf{R}.\end{aligned} \tag{10}$$

At NLL accuracy, by changing the color basis to the one in which $\mathbf{\Gamma}^{(1)}_{ij\to klB}$ is diagonal, the path ordered exponentials in Eq. (4) reduce to sum over simple exponentials. At NNLL accuracy, to recast the path ordered exponential of the soft anomalous dimension matrix in a form containing simple exponential functions, we make use of a technique detailed in e.g., [41,42] resulting in

$$\begin{aligned}&\mathbf{U}_R(N,Q^2,\{m^2\},\mu_{\mathrm{R}}^2)\\ &\quad=\left(\mathbf{1}+\frac{\alpha_{\mathrm{s}}(Q^2/\bar{N}^2)}{\pi}\mathbf{K}\right)\left[\left(\frac{\alpha_{\mathrm{s}}(\mu_{\mathrm{R}}^2)}{\alpha_{\mathrm{s}}(Q^2/\bar{N}^2)}\right)^{\frac{\vec{\lambda}^{(1)}}{2\pi b_0}}\right]_D\\ &\qquad\times\left(\mathbf{1}-\frac{\alpha_{\mathrm{s}}(\mu_{\mathrm{R}}^2)}{\pi}\mathbf{K}\right),\end{aligned} \tag{11}$$

with the subscript D indicating a diagonal matrix. The matrix $\mathbf{K}$ is given by

$$K_{IJ}=\delta_{IJ}\lambda_I^{(1)}\frac{b_1}{2b_0^2}-\frac{(\mathbf{\Gamma}_R^{(2)})_{IJ}}{2\pi b_0+\lambda_I^{(1)}-\lambda_J^{(1)}}, \tag{12}$$

where b_0 and b_1 are the first two coefficients of expansion β_{QCD} in α_{s},

$$b_0=\frac{11C_{\mathrm{A}}-4n_{\mathrm{f}}T_{\mathrm{R}}}{12\pi}, \tag{13}$$

$$b_1=\frac{17C_{\mathrm{A}}^2-n_{\mathrm{f}}T_{\mathrm{R}}(10C_{\mathrm{A}}+6C_{\mathrm{F}})}{24\pi^2}. \tag{14}$$

In our calculation we set $n_{\mathrm{f}}=5$.

In the diagonal basis of the one-loop soft anomalous dimension, up to NNLL accuracy Eq. (2) can be written as

$$\begin{aligned}&\frac{d\tilde{\tilde{\sigma}}^{(\mathrm{NNLL})}_{ij\to klB}}{dQ^2}(N,Q^2,\{m^2\},\mu_{\mathrm{R}}^2)\\ &\quad=\mathrm{Tr}[\mathbf{H}_R(Q^2,\{m^2\},\mu_{\mathrm{F}}^2,\mu_{\mathrm{R}}^2)\bar{\mathbf{U}}_R(N+1,Q^2,\{m^2\},Q^2)\\ &\qquad\times\tilde{\mathbf{S}}_{\mathbf{R}}(N+1,Q^2,\{m^2\})\mathbf{U}_R(N+1,Q^2,\{m^2\},Q^2)]\\ &\qquad\times\Delta^i(N+1,Q^2,\mu_{\mathrm{F}}^2,\mu_{\mathrm{R}}^2)\Delta^j(N+1,Q^2,\mu_{\mathrm{F}}^2,\mu_{\mathrm{R}}^2).\end{aligned} \tag{15}$$

In the above equation, the $\mathbf{H}_R$ and $\tilde{\mathbf{S}}_R$ are hard and soft function matrices projected onto R color basis. They are calculated at the NLO accuracy, i.e., including the $\mathcal{O}(\alpha_{\mathrm{s}})$ terms in Eqs. (3) and (5). The LO hard matrix is derived from the Born cross section. The NLO hard matrix contains nonlogarithmic contributions which are independent of N. They consist of virtual loop contributions, real terms of collinear origin and the contributions from the evolution matrices $\mathbf{U_R}$ and $\bar{\mathbf{U}}_{\mathbf{R}}$, corresponding to evolution between μ_{R} and Q, expanded up to $\mathcal{O}(\alpha_{\mathrm{s}})$. The color-decomposed virtual corrections are extracted from the calculations of the NLO cross section in the `PowHel` framework [13]. Aside from evolution terms, the remaining terms in $\mathbf{H}_R^{(1)}$ are obtained from the infrared-limit of the real corrections [43] using the method initially proposed in [44,45]. Additionally, we recalculate the one-loop soft function $\tilde{\mathbf{S}}^{(1)}$ [25,42]. The dependence on N in the soft function $\tilde{\mathbf{S}}_R$ enters only through the argument of α_{s} in Eq. (5).

Substituting the expression for the running coupling, we obtain up to NNLL accuracy for the soft matrix evolution factors in Eq. (15)

$$\begin{aligned}\mathbf{U}_R(N,Q^2,\{m^2\},Q^2)&=\left(\mathbf{1}+\frac{\alpha_{\mathrm{s}}(\mu_{\mathrm{R}}^2)}{\pi(1-2\lambda)}\mathbf{K}\right)[e^{g_s(N)\vec{\lambda}^{(1)}}]_D\\ &\quad\times\left(\mathbf{1}-\frac{\alpha_{\mathrm{s}}(\mu_{\mathrm{R}}^2)}{\pi}\mathbf{K}\right),\end{aligned} \tag{16}$$

$$\begin{aligned}\bar{\mathbf{U}}_R(N,Q^2,\{m^2\},Q^2)&=\left(\mathbf{1}-\frac{\alpha_{\mathrm{s}}(\mu_{\mathrm{R}}^2)}{\pi}\mathbf{K}^\dagger\right)[e^{g_s(N)(\vec{\lambda}^{(1)})^*}]_D\\ &\quad\times\left(\mathbf{1}+\frac{\alpha_{\mathrm{s}}(\mu_{\mathrm{R}}^2)}{\pi(1-2\lambda)}\mathbf{K}^\dagger\right),\end{aligned} \tag{17}$$

where

$$\begin{aligned}g_s(N)=\frac{1}{2\pi b_0}\{&\log(1-2\lambda)+\alpha_{\mathrm{s}}(\mu_{\mathrm{R}}^2)\left[\frac{b_1}{b_0}\frac{\log(1-2\lambda)}{1-2\lambda}\right.\\ &\left.-2\gamma_{\mathrm{E}}b_0\frac{2\lambda}{1-2\lambda}+b_0\log\left(\frac{Q^2}{\mu_{\mathrm{R}}^2}\right)\frac{2\lambda}{1-2\lambda}\right]\},\end{aligned} \tag{18}$$

and

$$\lambda=\alpha_{\mathrm{s}}(\mu_{\mathrm{R}}^2)b_0\log N. \tag{19}$$

The $\mathbf{U}_R$ and $\bar{\mathbf{U}}_R$ factors in Eqs. (16), (17) correspond to evolution from $Q/\bar{N}$ up to Q and depend on μ_{R} only through the argument α_{s}. The N-independent evolution from μ_{R} to Q is incorporated into the hard function, as noted earlier.

The other factors contributing to the resummation of logarithms, i.e., the radiative factors for the incoming partons, Δ^i and Δ^j are widely known. The results at NLL accuracy can be found for example in [39,46] and at the NNLL level in [40].

As already noted, at NLL accuracy, by changing the color basis to the R-basis, the path ordered exponentials in Eq. (4) reduce to simple exponentials. Equivalently, the NLL accuracy can be obtained by neglecting terms suppressed by a factor of α_{s} in Eqs. (16), (17) and (18). This results in the soft matrix evolution factors turning into exponential functions for the eigenvalues of the soft anomalous dimension matrix. At NLL, it is also enough

to only know the LO contributions to the hard and soft function, which results in the following expression for the resummed cross section in the Mellin space:

$$\begin{aligned}\frac{d\tilde{\tilde{\sigma}}^{(\mathrm{NLL})}_{ij\to klB}}{dQ^2}(N,Q^2,\{m^2\},\mu_\mathrm{F}^2,\mu_\mathrm{R}^2)&=\mathbf{H}^{(0)}_{R,IJ}(Q^2,\{m^2\})\tilde{\mathbf{S}}^{(0)}_{R,JI}\\&\times\Delta^i(N+1,Q^2,\mu_\mathrm{F}^2,\mu_\mathrm{R}^2)\Delta^j(N+1,Q^2,\mu_\mathrm{F}^2,\mu_\mathrm{R}^2)\\&\times\exp\left[\frac{\log(1-2\lambda)}{2\pi b_0}((\lambda_J^{(1)})^*+\lambda_I^{(1)})\right],\end{aligned}\tag{20}$$

where the color indices I and J are implicitly summed over. The trace of the product of two matrices $\mathbf{H_R}^{(0)}$ and $\tilde{\mathbf{S}}^{(0)}_R$ returns the LO cross section. The incoming parton radiative factors Δ_i are now considered only at NLL accuracy.

In order to improve the accuracy of the numerical approximation provided by resummation, it is customary to include terms up to $\mathcal{O}(\alpha_\mathrm{s})$ in the expansion of the hard and soft function leading to

$$\begin{aligned}\frac{d\tilde{\tilde{\sigma}}^{(\mathrm{NLLw}\mathcal{C})}_{ij\to klB}}{dQ^2}(N,Q^2,\{m^2\},\mu_\mathrm{F}^2,\mu_\mathrm{R}^2)&=\mathbf{H}_{R,IJ}(Q^2,\{m^2\},\mu_\mathrm{F}^2,\mu_\mathrm{R}^2)\tilde{\mathbf{S}}_{R,JI}(Q^2,\{m^2\})\\&\times\Delta^i(N+1,Q^2,\mu_\mathrm{F}^2,\mu_\mathrm{R}^2)\Delta^j(N+1,Q^2,\mu_\mathrm{F}^2,\mu_\mathrm{R}^2)\\&\times\exp\left[\frac{\log(1-2\lambda)}{2\pi b_0}((\lambda_J^{(1)})^*+\lambda_I^{(1)})\right],\end{aligned}\tag{21}$$

where

$$\mathbf{H}_R\tilde{\mathbf{S}}_R=\mathbf{H}_R^{(0)}\tilde{\mathbf{S}}_R^{(0)}+\frac{\alpha_\mathrm{s}}{\pi}[\mathbf{H}_R^{(1)}\tilde{\mathbf{S}}_R^{(0)}+\mathbf{H}_R^{(0)}\tilde{\mathbf{S}}_R^{(1)}].$$

We will refer to this result as "NLL w $\mathcal{C}$", since the N-independent $\mathcal{O}(\alpha_\mathrm{s})$ terms in the hard and soft function are often collected together in one function, known as the hard matching coefficient, $\mathcal{C}$. Although we choose to treat these terms as in Eq. (21), we keep the name "w $\mathcal{C}$" ("w" standing for "with") as a useful shorthand.

The resummation-improved cross sections for the $pp\to t\bar{t}H$ process are obtained through matching the resummed expressions with the full NLO cross sections

$$\begin{aligned}\frac{d\sigma^{(\mathrm{matched})}_{h_1h_2\to klB}}{dQ^2}(Q^2,\{m^2\},\mu_\mathrm{F}^2,\mu_\mathrm{R}^2)&=\frac{d\sigma^{(\mathrm{NLO})}_{h_1h_2\to klB}}{dQ^2}(Q^2,\{m^2\},\mu_\mathrm{F}^2,\mu_\mathrm{R}^2)\\&+\frac{d\sigma^{(\mathrm{res\text{-}exp})}_{h_1h_2\to klB}}{dQ^2}(Q^2,\{m^2\},\mu_\mathrm{F}^2,\mu_\mathrm{R}^2)\end{aligned}\tag{22}$$

with

$$\begin{aligned}\frac{d\sigma^{(\mathrm{res\text{-}exp})}_{h_1h_2\to klB}}{dQ^2}(Q^2,\{m^2\},\mu_\mathrm{F}^2,\mu_\mathrm{R}^2)&=\sum_{i,j}\int_\mathsf{C}\frac{dN}{2\pi i}\rho^{-N}f_{i/h_1}^{(N+1)}(\mu_\mathrm{F}^2)f_{j/h_2}^{(N+1)}(\mu_\mathrm{F}^2)\\&\times\left[\frac{d\tilde{\tilde{\sigma}}^{(\mathrm{res})}_{ij\to klB}}{dQ^2}(N,Q^2,\{m^2\},\mu_\mathrm{F}^2,\mu_\mathrm{R}^2)\right.\\&\left.-\frac{d\tilde{\tilde{\sigma}}^{(\mathrm{res})}_{ij\to klB}}{dQ^2}(N,Q^2,\{m^2\},\mu_\mathrm{F}^2,\mu_\mathrm{R}^2)|_{(\mathrm{NLO})}\right],\end{aligned}\tag{23}$$

where "matched" can stand for "NLO + NNLL", "NLO + NLL" or "NLO + NLL w $\mathcal{C}$" and "res" for "NNLL", "NLL" or "NLL w $\mathcal{C}$", correspondingly. The inclusive cross section is obtained by integrating the invariant mass distribution given in Eq. (15) over Q^2 and $\hat{\sigma}^{(\mathrm{res})}_{ij\to klB}(N,\mu_\mathrm{F}^2,\mu_\mathrm{R}^2)|_{(\mathrm{NLO})}$ represents its perturbative expansion truncated at NLO. The moments of the parton distribution functions (pdf) $f_{i/h}(x,\mu_\mathrm{F}^2)$ are defined in the standard way

$$f_{i/h}^{(N)}(\mu_\mathrm{F}^2)\equiv\int_0^1 dx x^{N-1}f_{i/h}(x,\mu_\mathrm{F}^2).$$

The inverse Mellin transform (23) is evaluated numerically using a contour C in the complex-N space according to the "minimal prescription" method developed in Ref. [39].[4]

Besides the resummed cross sections we also compute approximate NNLO cross sections. We obtain them from an explicit expansion of the resummed cross section given by Eq. (15) up to the NNLO accuracy, followed by the inverse Mellin transform of the NNLO terms performed analytically. The resulting momentum-space expressions are implemented numerically and added to the full NLO cross sections, thus yielding approximate NNLO predictions. In what follows the acronym $\mathrm{NNLO_{Approx}}$ will be used for these results.

III. NUMERICAL RESULTS FOR THE $pp\to t\bar{t}H$ PROCESS AT NLO + NNLL ACCURACY

In this section we present and discuss our state-of-the-art NLO + NNLL predictions for the $t\bar{t}H$ production process at the LHC for the two collision energies $\sqrt{S}=13$ TeV and $\sqrt{S}=14$ TeV. The results for the total cross section which we present below are obtained by integrating out the invariant mass distribution over the invariant mass Q. The distribution in Q undergoes resummation of soft gluon

[4]Note that the application of the minimal prescription method has been disputed in the literature, especially in the context of heavy quark pair production [47,48]. For a detailed comparison of numerical results obtained with various resummation techniques we refer the reader to e.g., Ref. [49].

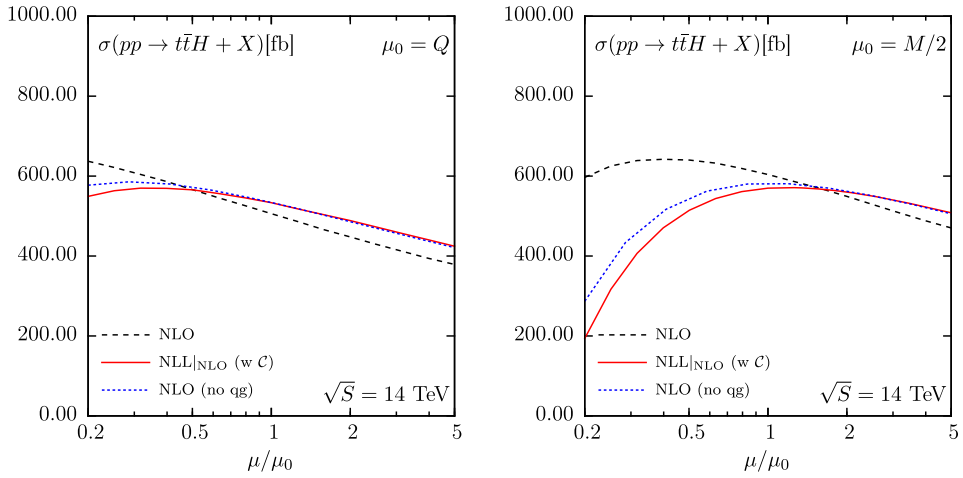

FIG. 1. Comparison between the expansion of the resummed expression Eq. (15) up to the NLO accuracy in α_s, the full NLO result and the NLO result without the qg channel contribution as a function of the scale $\mu = \mu_F = \mu_R$.

corrections in the threshold limit $\hat{s} \to Q^2$, i.e., in the invariant mass kinematics. This approach is different from directly resumming corrections to the total cross section in the absolute threshold limit $\hat{s} \to M^2$, which we performed in [23]. Numerical results involving resummation are obtained using two independently developed in-house computer codes. The same applies to the implementattion of the approximated NNLO results, $\text{NNLO}_{\text{Approx}}$. Apart from NLL and NNLL predictions matched to the NLO according to Eq. (22), we also show the NLL predictions supplemented with the $\mathcal{O}(\alpha_s)$ nonlogarithmic contributions ("NLL w $\mathcal{C}$"), also matched to the NLO, as well as the $\text{NNLO}_{\text{Approx}}$ cross sections.

In the phenomenological analysis we use $m_t = 173$ GeV and $m_H = 125$ GeV. The NLO cross section is calculated using the aMC@NLO code [50]. We perform the current analysis employing PDF4LHC15_100 sets [51–56] and use the corresponding values of α_s. In particular, for the NLO + NLL predictions we use the NLO sets, whereas the NLO + NNLL and $\text{NNLO}_{\text{Approx}}$ predictions are calculated with NNLO sets. For the sake of comparison with Broggio *et al.* [28], we adopt the same choice of pdfs, i.e., MMHT2014 [53].

We present most of our analysis for two choices of the central values of the renormalization and factorization scales: $\mu_0 = \mu_{F,0} = \mu_{R,0} = Q$ and $\mu_0 = \mu_{F,0} = \mu_{R,0} = M/2$. The former choice is motivated by the invariant mass Q being the natural scale for the invariant mass kinematics used in resummation. The latter choice of the scale is often made in the NLO calculations of the total cross section reported in the literature, see e.g., [20]. By studying results for these two relatively distant scales, we aim to cover a span of scale choices relevant in the problem. The theoretical error due to scale variation is calculated using the so-called 7-point method, where the minimum and maximum values obtained with $(\mu_F/\mu_0, \mu_R/\mu_0) = (0.5, 0.5), (0.5, 1), (1, 0.5), (1, 1), (1, 2), (2, 1), (2, 2)$ are considered. For reasons of technical simplicity, the pdf error is calculated for the NLO predictions; however we expect that adding the soft gluon corrections only minimally influences the value of the pdf error.

As discussed in the previous section for the evaluation of the first-order hard function matrix $\mathbf{H}_{IJ}^{(1)}$ we need to know one-loop virtual corrections to the process, decomposed into various color transitions IJ. We extract them numerically using the publicly available `PowHel` implementation of the $t\bar{t}H$ process [13]. In particular, we use analytical relations to translate between virtual corrections split into various color configurations in the color flow basis used in [13] and our default singlet-octet(s) bases. We cross-check the consistency of results obtained in this way by comparing the color-summed one-loop virtual contributions to $\text{Tr}[\mathbf{H}^{(1)}\tilde{\mathbf{S}}^{(0)}]$ with the full one-loop virtual correction given by the `PowHel` package [13], as well as the `POWHEG` implementation of the $t\bar{t}H$ process [14] and the standalone MadLoop implementation in `aMC@NLO` [11].

We begin the discussion of numerical results by analyzing how well the full NLO result for the total cross section is approximated by the expansion of the resummed cross section up to the same accuracy in α_s as in NLO. It was first pointed out in [25] in the context of the $t\bar{t}W$ production and then later in [26] for the $t\bar{t}H$ process that the qg production channel carries a relatively large numerical significance, especially in relation to the scale uncertainty. This is due to the fact that a nonzero contribution from the qg channel appears first at NLO; i.e., it is subleading with respect to contributions from the $q\bar{q}$ and gg channels. Correspondingly, no resummation is performed for this channel, and it enters the matched resummation-improved formula Eq. (22) only through a fixed order contribution at NLO. It is then clear that in order to estimate how much of the NLO result is constituted by the terms accounted for in

TABLE I. Total cross section predictions for $pp \to t\bar{t}H$ at various LHC collision energies and central scale choices. The listed error is the theoretical error due to the scale variation calculated using the 7-point method.

		$\sigma(pp \to t\bar{t}H)$ [fb]				
$\sqrt{S}$ [TeV]	μ_0	NLO	NLO + NLL	NLO + NLL (w $\mathcal{C}$)	$\text{NNLO}_{\text{Approx}}$	NLO + NNLL
13	Q	$418^{+11.9\%}_{-11.7\%}$	$439^{+9.8\%}_{-9.2\%}$	$484^{+8.2\%}_{-8.5\%}$	$484^{+6.6\%}_{-7.5\%}$	$499^{+7.6\%}_{-6.9\%}$
	$Q/2$	$468^{+9.8\%}_{-10.7\%}$	$477^{+8.6\%}_{-8.0\%}$	$496^{+6.0\%}_{-7.2\%}$	$485^{+6.2\%}_{-8.2\%}$	$498^{+6.0\%}_{-6.3\%}$
	$M/2$	$499^{+5.9\%}_{-9.3\%}$	$504^{+8.1\%}_{-7.8\%}$	$505^{+5.7\%}_{-6.1\%}$	$483^{+7.0\%}_{-8.8\%}$	$502^{+5.3\%}_{-6.0\%}$
14	Q	$506^{+11.8\%}_{-11.5\%}$	$530^{+9.8\%}_{-9.2\%}$	$585^{+8.3\%}_{-8.5\%}$	$584^{+6.5\%}_{-7.5\%}$	$603^{+7.8\%}_{-6.9\%}$
	$Q/2$	$566^{+9.9\%}_{-10.6\%}$	$576^{+8.7\%}_{-8.0\%}$	$599^{+6.2\%}_{-7.3\%}$	$585^{+6.4\%}_{-8.3\%}$	$602^{+6.0\%}_{-6.4\%}$
	$M/2$	$604^{+6.1\%}_{-9.2\%}$	$609^{+8.4\%}_{-7.8\%}$	$611^{+6.0\%}_{-6.3\%}$	$583^{+7.3\%}_{-8.8\%}$	$607^{+5.7\%}_{-6.1\%}$

the resummed expression, Eq. (15), its expansion should not be directly compared with full NLO but with NLO cross section without a contribution from the qg channel. We obtain the latter result from the `PowHel` package [13]. Its comparison with the expansion of the resummed expression in Eq. (15) up to NLO accuracy in α_s as a function of the scale $\mu = \mu_F = \mu_R$ is shown in Fig. 1 for $\sqrt{S} = 14$ TeV and two choices of the central scale $\mu_0 = Q$ and $\mu_0 = M/2$. While in both cases the expansion of the resummed cross section differs significantly from the full NLO, the NLO result with the qg channel contribution subtracted is much better approximated by the expansion, especially for the dynamical scale choice $\mu = Q$ and for the fixed scale choice $\mu \geq M/2$, for the physically motivated scale choices. Such good agreement lets us conclude that the NNLL resummed formula will indeed take into account a prevailing part of the higher-order contributions from the $q\bar{q}$ and gg channels to all orders in α_s.[5]

Our numerical predictions for the total cross sections at $\sqrt{S} = 13$ TeV and $\sqrt{S} = 14$ TeV are shown in Table I. We report results obtained with our default scale choice $\mu_0 = Q$ as well as the fixed scale $\mu_0 = M/2$. Additionally, we also provide results for the "in-between" choice of $\mu_0 = Q/2$. While for these choices of central scale the NLO results vary by 20%, the variation[6] reduces as the accuracy of resumation increases. In particular, the NLO + NNLL results show a remarkable stability with respect to the scale choice. We also observe that the 7-point method scale uncertainty of the results gets reduced with the increasing accuracy. In particular, for all scale choices, the scale uncertainty of the NLO + NNLL cross section is reduced compared to the NLO scale uncertainty calculated in the same way. The degree up to which the scale uncertainty is reduced depends on the specific choice of the central scale. For example, for $\mu_0 = Q/2$ the theoretical precision of the NLO + NNLL prediction is improved by about 40% with respect to the NLO result, bringing the scale error calculated with the 7-point method down to less than 6.5% of the central cross section value. We also provide the approximate NNLO results ($\text{NNLO}_{\text{Approx}}$). We find them to be fully consistent with the NLO + NNLL results. For the scales choices considered in Table I, the $\text{NNLO}_{\text{Approx}}$ predictions are slightly lower than NLO + NNLL results, indicating a small positive contribution from logarithmic terms beyond NNLO. The $\text{NNLO}_{\text{Approx}}$ results are also stable with respect to scale variation, with the theoretical uncertainty somewhat larger than for the NLO + NNLL results, as can be expected. We have checked that our $\text{NNLO}_{\text{Approx}}$ cross sections agree very well with the corresponding predictions obtained in Ref. [28]. The results shown in Table I are further graphically presented in Fig. 2.

The size of the K_{NNLL} factor measuring the impact of the higher-order logarithmic corrections, defined as the ratio of the NLO + NNLL to NLO cross sections, is shown in Table II. It varies depending on the value of the central scale. The variation is almost entirely driven by the scale dependence of the NLO cross section. For the choice $\mu_0 = Q$ the K_{NNLL}-factor can be as high as 1.19.

Given the conspicuous stability of the NLO + NNLL results, see Fig. 2, we are encouraged to combine our results obtained for various scale choices. For this purpose we adopt the method proposed by the Higgs Cross Section Working Group [20]. In this way, we obtain for the $t\bar{t}H$ cross section at 13 TeV

$$\sigma_{\text{NLO+NNLL}} = 500^{+7.5\%+3.0\%}_{-7.1\%-3.0\%} \text{ fb},$$

and at 14 TeV

$$\sigma_{\text{NLO+NNLL}} = 604^{+7.6\%+2.9\%}_{-7.1\%-2.9\%} \text{ fb},$$

where the first error is the theoretical uncertainty due to scale variation and the second error is the pdf uncertainty.

[5]Although the expansion and the NLO results without the qg channel contribution agree very well at this level of accuracy in α_s, since we do not know the second-order hard-matching coefficients we cannot expect an equally good approximation of the NNLO result by the expansion of the NNLL formula.

[6]The value of 10% scale error often quoted in the literature relates to a variation by factors of 0.5 or 2 around $\mu_0 = M/2$, while here we consider a much wider range between $M/2$ and Q.

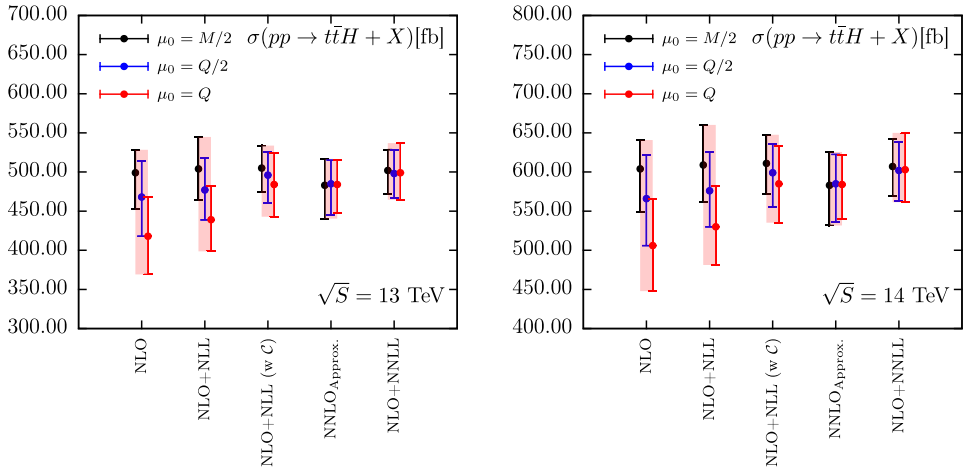

FIG. 2. Graphical illustration of results presented in Table I.

Our findings are further illustrated in the plots in Figs. 3 and 4. We show there the scale dependence of $t\bar{t}H$ total cross sections calculated with the factorization and renormalization scale kept equal, $\mu = \mu_F = \mu_R$ for two LHC collision energies $\sqrt{S} = 13$ TeV and $\sqrt{S} = 14$ TeV. As readily expected, apart from quantitative differences there is no visible disparity between the qualitative behavior of results for the two energies. For the central scale choice of $\mu_0 = Q$, we observe a steady increase in the stability of the cross section value with respect to scale variation as the accuracy of resummation improves from NLO + NLL to NLO + NNLL. Our final NLO + NNLL prediction is characterized by a very low scale dependence if $\mu_F = \mu_R$ choice is made. Correspondingly, if calculated only along the $\mu_F = \mu_R$ direction, the theoretical error on the NLO + NNLL prediction due to scale variation would be at the level of 1%, which is a significant reduction from the 10% variation of the NLO, c.f. Table I. Results obtained with the scale choice of $\mu_0 = M/2$ behave mostly in a similar way. Only in the very low scale regime, $\mu \lesssim 0.2M$, the NLO + NNLL cross section shows a stronger scale dependence. For this scale choice, the rise of the matched resummed predictions with the diminishing scale is driven by the fall of the expanded resummed $\text{NLL}|_{\text{NLO}}$ results, cf. Fig. 1, and therefore is a consequence of the relatively large scale dependence of NLO contributions stemming from the qg channel.

TABLE II. Total cross section predictions at NLO + NNLL for $pp \to t\bar{t}H$ at various LHC collision energies and central scale choices. The first error is the theoretical error due to the scale variation calculated using the 7-point method, and the second is the pdf error.

$\sqrt{S}$ [TeV]	μ_0	NLO + NNLL [fb]	K_{NNLL} factor
13	Q	$499^{+7.6\%+2.9\%}_{-6.9\%-2.9\%}$	1.19
	$Q/2$	$498^{+6.0\%+3.0\%}_{-6.3\%-3.0\%}$	1.06
	$M/2$	$502^{+5.3\%+3.1\%}_{-6.0\%-3.1\%}$	1.01
14	Q	$603^{+7.8\%+2.8\%}_{-6.9\%-2.8\%}$	1.22
	$Q/2$	$602^{+6.0\%+2.9\%}_{-6.4\%-2.9\%}$	1.06
	$M/2$	$607^{+5.7\%+3.0\%}_{-6.1\%-3.0\%}$	1.01

Furthermore, in Figs. 3 and 4 we display the scale dependence of the $\text{NNLO}_{\text{Approx}}$ cross sections. The $\text{NNLO}_{\text{Approx}}$ results are rather close to the ones at the NLO + NNLL and NLO + NLL (w $\mathcal{C}$) accuracy, with somewhat more noticeable deviations at smaller scales. We also observe that apart from the region of very low unphysical scales $\mu = \mu_R = \mu_F$, the NLO + NNLL predictions are slightly higher than the $\text{NNLO}_{\text{Approx}}$ predictions, in accordance with results listed in Table I. At larger scales, one notices that the $\text{NNLO}_{\text{Approx}}$ and NLO + NLL (w $\mathcal{C}$) curves nearly overlap. We have checked that this effect is a numerical coincidence. Firstly, the two predictions have different functional dependence on $\alpha_s(\mu)$, $\log N$ and $\log \mu$. Secondly, the effect is neither sustained at scales higher than $\mu = 5Q$, nor present when the dependence on μ_F or μ_R is analyzed separately, see Fig. 5 and Fig. 6.

We further investigate the dependence on the scale but showing separately the renormalization and factorization scale dependence while keeping the other scale fixed. Figure 5 shows the dependence on μ_R and Fig. 6 on μ_F for the $\sqrt{S} = 14$ TeV. We conclude that the weak scale dependence present when the scales are varied simultaneously is a result of the opposite behavior of the total cross section under μ_F and μ_R variations. The effect is similar to the cancellations between renormalization and factorization scale dependencies for threshold resummation in the absolute threshold limit which we observed in [23]. The typical decrease of the cross section with increasing μ_R originates from running of α_s. The behavior under the variation of the factorization scale, on the other hand, is related to the effect of scaling violation of pdfs at probed values of x. In this context, it is interesting to observe that

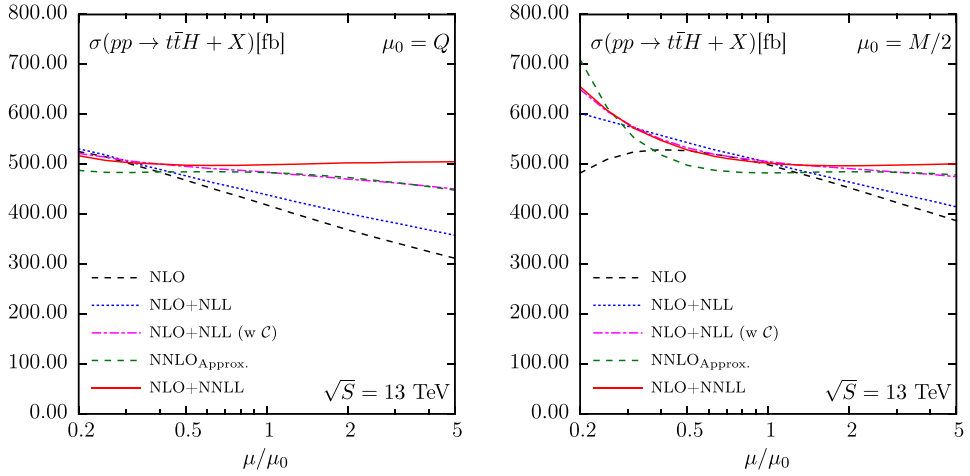

FIG. 3. Scale dependence of the total cross section for the process $pp \to t\bar{t}H$ at the LHC with $\sqrt{S} = 13$ TeV. Results shown for the choice $\mu = \mu_{\rm F} = \mu_{\rm R}$ and two central scale values $\mu_0 = Q$ (left plot) and $\mu_0 = M/2$ (right plot).

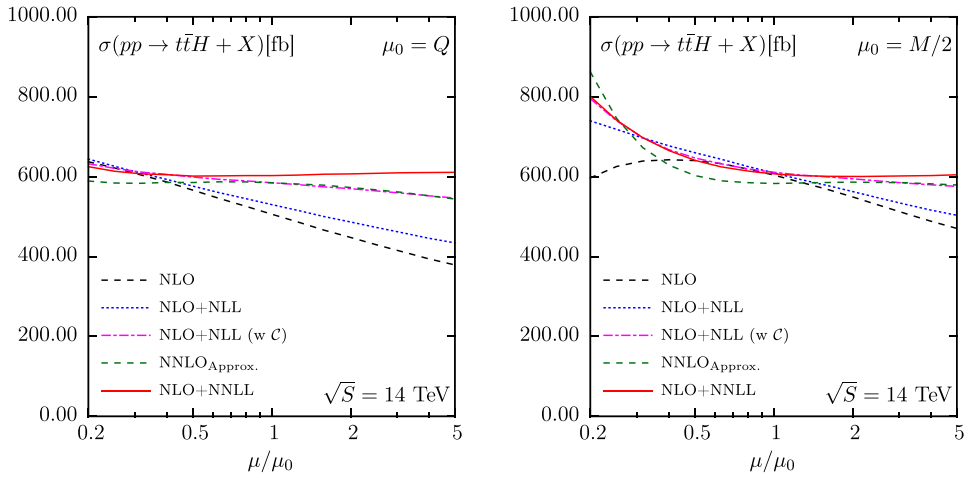

FIG. 4. Scale dependence of the total cross section for the process $pp \to t\bar{t}H$ at the LHC with $\sqrt{S} = 14$ TeV. Results shown for the choice $\mu = \mu_{\rm F} = \mu_{\rm R}$ and two central scale values $\mu_0 = Q$ (left plot) and $\mu_0 = M/2$ (right plot).

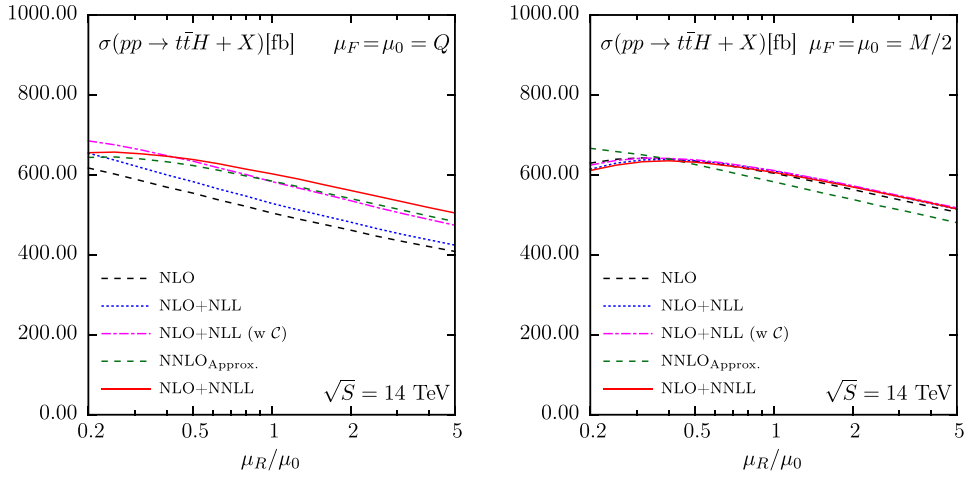

FIG. 5. Renormalization scale dependence of the total cross section for the process $pp \to t\bar{t}H$ at the LHC with $\sqrt{S} = 14$ TeV and $\mu_{\rm F} = \mu_{\rm F,0}$ kept fixed. Results shown two central scale choices $\mu_0 = \mu_{\rm F,0} = \mu_{\rm R,0} = Q$ (left plot) and $\mu_0 = \mu_{\rm F,0} = \mu_{\rm R,0} = M/2$ (right plot).

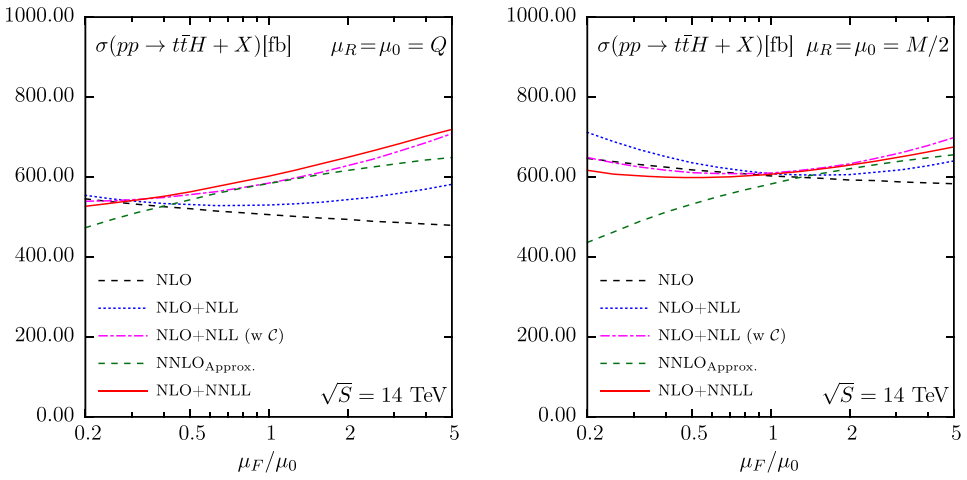

FIG. 6. Factorization scale dependence of the total cross section for the process $pp \to t\bar{t}H$ at the LHC with $\sqrt{S} = 14$ TeV and $\mu_R = \mu_{R,0}$ kept fixed. Results shown two central scale choices $\mu_0 = \mu_{F,0} = \mu_{R,0} = Q$ (left plot) and $\mu_0 = \mu_{F,0} = \mu_{R,0} = M/2$ (right plot).

the NLO + NLL predictions in Fig. 6 show very little μ_F dependence around the central scale, in agreement with expectation of the factorization scale dependence in the resummed exponential and in the pdfs canceling each other, here up to NLL. The relatively strong dependence on μ_F of the NLO + NLL (w $\mathcal{C}$) predictions can be then easily understood: the resummed expression will take into account higher-order scale-dependent terms which involve higher-order terms of both logarithmic (in N) and nonlogarithmic origin. The latter terms do not have their equivalent in the pdf evolution since the pdfs do not carry any process-specific information. Correspondingly, the μ_F dependence does not cancel and can lead to strong effects if the nonlogarithmic terms are numerically significant. Figures 5 and 6 also demonstrate explicitly that the apparent similarity of the $\text{NNLO}_{\text{approx}}$ and the NLO + NLL (w $\mathcal{C}$) results for $\mu = \mu_F = \mu_R$ at large values of μ is a pure numerical coincidence, as the two curves are visibly separated in this region when only a variation of μ_F or μ_R is performed. A somewhat larger difference between the two results shown for $\mu_R = M/2$ in Fig. 6 occurs in the region where μ_F is very small in comparison with the typical invariant mass $Q \sim 2.64M$ [28], and consequently corresponds to scale choices which are not well motivated physically.

Given apparent cancellations between μ_R and μ_F scale dependence, we believe that the 7-point method of estimating the scale error, allowing for an independent variation of μ_R only (for $\mu_F = \mu_0$), is better suited here as an estimate of the theory error than the often used variation of $\mu = \mu_F = \mu_R$. Another reason for our preference of this conservative estimate is presence of the hard and soft functions in the resummation formula, Eq. (15), which involve virtual corrections and are known only up to the order α_s. Due to suppression of the LO phase space, they provide a relatively significant part of the NLO + NNLL corrections to the total cross sections, cf. Table I. It is then justified to suppose that a similar situation might take place also at higher logarithmic orders and that the value of the yet unknown two-loop virtual corrections which feed into the second-order coefficients in Eq. (15) can have a nonnegligible impact on the predictions. With the 7-point method error estimate, we expect that this effect is included within the size of the error.

Our observation of stability of the predictions with respect to the scale variation is also confirmed at the differential level. In Fig. 7 we show the differential distribution in the invariant mass Q of the $t\bar{t}H$ system produced at $\sqrt{S} = 14$ TeV. While the NLO distributions calculated with $\mu_0 = Q$ and $\mu_0 = M/2$ differ visibly, the NLO + NNLL distributions for these scale choices are very close in shape and value. The stability of the NLO + NNLL distribution with respect to the scale choice is demonstrated explicitly in Fig. 8. Correspondingly, the ratios of the NLO + NNLL to NLO distributions differ. In particular for the choice of $\mu_0 = Q$ the NNLL differential K-factor grows with the invariant mass and can be higher than 1.2 at large Q. The scale error for the invariant mass distribution is also calculated using the 7-point method. The error bands are slightly narrower for the NLO + NNLL distributions than at NLO. If the scale errors were calculated by variation of $\mu = \mu_F = \mu_R$ by factors of 0.5 and 2, the NLO + NNLL error bands would be considerably narrower.

We complete this part of the discussion by comparing resummed results obtained using the invariant mass kinematics with those obtained earlier by us in the absolute mass threshold limit [23]. At 13 (14) TeV, our most accurate prediction in these kinematics, i.e., the NLO + NLL cross section including the first-order hard-matching coefficient, evaluated with PDF4LHC15_100 pdf sets, amounted to $\sigma_{\text{NLO+NLLw}\mathcal{C}} = 530^{+7.8\%}_{-5.5\%}(641^{+7.9\%}_{-5.5\%})$. The absolute mass threshold approach allows only for a fixed scale

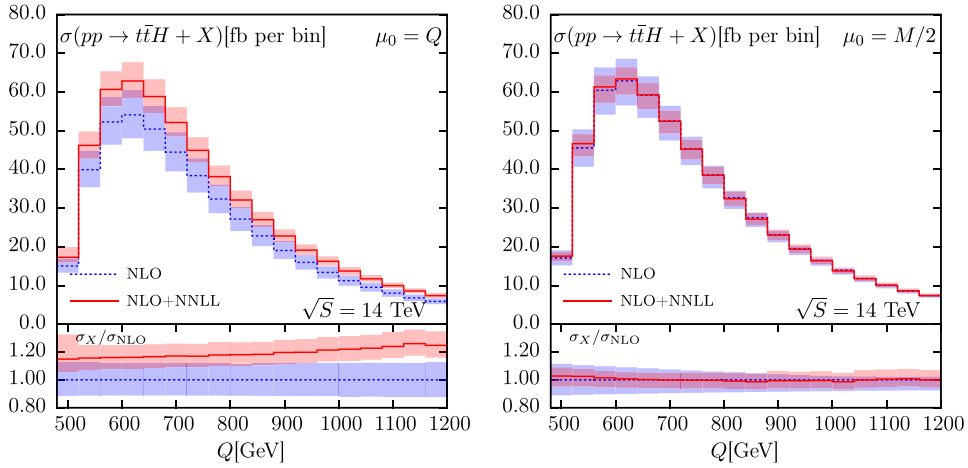

FIG. 7. Comparison of the NLO + NNLL and NLO invariant mass distributions for the process $pp \to t\bar{t}H$ at the LHC with $\sqrt{S} = 14$ TeV. Results shown for two central scale choices $\mu_0 = Q$ (left plot) and $\mu_0 = M/2$ (right plot). Lower panels show the ratio of the distributions with respect to the NLO predictions.

choice, which is taken to be $\mu_0 = \mu_{\rm F} = \mu_{\rm R} = M/2$. Comparing this result with our NLO + NLL predictions for the same scale choice in the invariant mass kinematics, cf. Table I, we see that the results calculated using the two resummation methods agree within errors.

In the remaining part of this section we comment on the relation of our results to the results of Broggio *et al.* [28]. That work relies on a resummation formula derived in the SCET framework in [26], though for the purpose of numerical calculations the Mellin space is adopted. In order to facilitate a comparison with results of [28] we recalculate our results as a function of the scale $\mu = \mu_{\rm F} = \mu_{\rm R}$ using MMHT2014 pdfs as in [28]. The outcome is presented in Fig. 9, where we show the NLO cross section and the matched resummed cross sections at various accuracy as a function of $\mu = \mu_{\rm F} = \mu_{\rm R}$ for the range of scales same as in Fig. 1 of [28]. Comparing the two figures, we find a qualitatively similar behavior of the NLO + NNLL cross sections as a function of the scale. Likewise, we obtain bigger NNLL corrections for the $\mu_0 = \mu_{\rm F} = \mu_{\rm R} = Q$ scale choice than for $\mu_0 = \mu_{\rm F} = \mu_{\rm R} = Q/2$. However, our NLO + NNLL results appear to be more stable with respect to the scale variation, leading to very little difference between the predictions for $\mu_0 = Q/2$ and $\mu_0 = Q$ (cf. also Table I). Figure 9 additionally illustrates another feature of our results, namely that for physically relevant values of $\mu_0 \gtrsim 0.3Q$ the scale dependence diminishes as the accuracy of the predictions increases, independently of the choice of the central scale μ_0.

However, it has to be noted that the scale choices made to obtain results reported in this paper and [28] are not equivalent. While our resummed expressions depend on

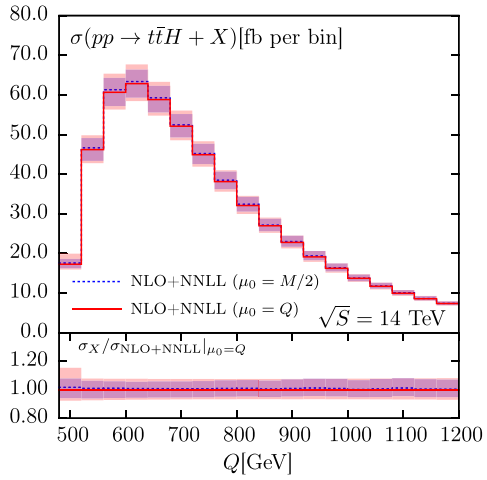

FIG. 8. Comparison of the NLO + NNLL invariant mass distributions for the process $pp \to t\bar{t}H$ at the LHC with $\sqrt{S} = 14$ TeV calculated with $\mu_0 = Q$ and $\mu_0 = M/2$. Lower panel shows the ratio to the NLO + NNLL distribution with $\mu_0 = Q$.

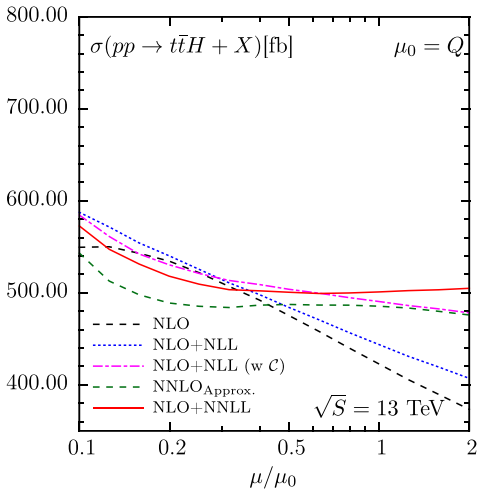

FIG. 9. Scale dependence of the total cross section for the process $pp \to t\bar{t}H$ at the LHC with $\sqrt{S} = 13$ TeV, calculated using MMHT 2014 pdfs. Results shown for the choice $\mu = \mu_{\rm F} = \mu_{\rm R}$ and the central scale value $\mu_0 = Q$.

μ_F and μ_R, the formulas used in [28] contain a dependence on the hard and soft scales μ_h and μ_s, as well as μ_F. The μ_s scale in [28] is chosen in such a way as to mimic the scale of soft radiation in the Mellin-space framework, i.e., $\mu_s = Q/\bar{N}$. Furthermore, for a given μ_F the resummed central results of [28] are obtained with a fixed hard scale $\mu_h = Q$, while the exact and approximate NLO results are evaluated keeping all other scales equal to the factorization scale. There is one choice of factorization scale for which the scale setting procedure of [28] corresponds to simultaneous variation of $\mu = \mu_F = \mu_R$, that is $\mu_F = Q$. For this choice we obtain $\sigma_{\mathrm{NLO+NNLL}} = 501.7^{+38.6}_{-34.6}$ fb, to be compared with $514.3^{+42.9}_{-39.5}$ fb reported in [28]; i.e., the central results of the two calculations agree within 2.5%. (The scale errors given together with the central values are expected to vary due to the different methods used for calculating them.) At NLO + NLL accuracy we do not find an agreement with [28]. We conclude that the differences in the properties of the NLO + NNLL cross sections reported here and in [28] are likely related to handling of scale setting in the two resummation approaches.

IV. SUMMARY

In this work, we have investigated the impact of the soft gluon emission effects on the total cross section for the process $pp \to t\bar{t}H$ at the LHC. The resummation of soft gluon emission has been performed using the Mellin-moment resummation technique at the NLO + NNLL accuracy in the three particle invariant mass kinematics. We have considered the differential distribution in the invariant mass as well as the total cross section, obtained by integrating the distribution. Our NLO + NNLL predictions are very stable with respect to a choice of the central scale μ_0 for the invariant mass distribution and consequently also for the total cross section. As this is not the case for the NLO predictions, the NNLL corrections vary in size, depending on the choice of the scale. In general, for the energies and scale choices considered they provide a non-negative modification of the cross section, which for the scale choice of $\mu_0 = Q$ can be even higher than 20% at larger values of Q^2.

We estimate the theoretical error due to scale variation by using the 7-point method, allowing for the independent variation of renormalization and factorization scales. The overall size of the theoretical scale error becomes gradually smaller as the accuracy of resummation increases, albeit the reduction is relatively modest. The reduction would have been much more significant if the scale error had been estimated by simultaneous variation of renormalization and factorization scales, i.e., of $\mu = \mu_F = \mu_R$. However, as it seems that the reduction in this case is a result of cancellations between factorization and renormalization scale dependencies, we choose a more conservative 7-point approach for estimating the error.

The stability of NLO + NNLL results with respect to the scale choice allows us to derive our best prediction for the $pp \to t\bar{t}H$ total cross section at 13 TeV

$$\sigma_{\mathrm{NLO+NNLL}} = 500^{+7.5\%+3.0\%}_{-7.1\%-3.0\%}\ \mathrm{fb},$$

and at 14 TeV

$$\sigma_{\mathrm{NLO+NNLL}} = 604^{+7.6\%+2.9\%}_{-7.1\%-2.9\%}\ \mathrm{fb},$$

where the first error is the theoretical uncertainty due to scale variation and the second error is the pdf uncertainty. The corresponding approximated NNLO results read at 13 TeV

$$\sigma_{\mathrm{NNLO_{Approx}}} = 484^{+6.8\%+3.0\%}_{-9.0\%-3.0\%}\ \mathrm{fb},$$

and at 14 TeV

$$\sigma_{\mathrm{NNLO_{Approx}}} = 584^{+7.1\%+2.9\%}_{-9.0\%-2.9\%}\ \mathrm{fb}.$$

They are thus somewhat lower than the NLO + NNLL predictions, with slightly larger errors. Both sets of results clearly agree very well within errors. We also note that the NLO + NNLL predictions are very close in their central value to the corresponding NLO predictions obtained for the scale choice $\mu_0 = M/2$ and are compatible with them within errors, vindicating the appropriateness of this commonly made choice. However, in comparison with the NLO predictions obtained in this way, our NLO + NNLL predictions are characterized by the overall smaller size of the theory error related to scale variation. For an equivalent scale choice setup, our NLO + NNLL results for the $t\bar{t}H$ production process at the LHC agree with the results previously obtained by Broggio *et al.* [28].

ACKNOWLEDGMENTS

We are grateful to M. Krämer for providing us with a numerical code for NLO $t\bar{t}H$ cross section calculations [9]. We would like to thank Daniel Schwartländer for his input in the later stages of this work. A. K gratefully acknowledges valuable exchanges with A. Kardos and Z. Trocsanyi. This work has been supported in part by the DFG Grant No. KU 3103/1. Support of the Polish National Science Center Grant No. DEC-2014/13/B/ST2/02486 is kindly acknowledged. This work was also partially supported by the U.S. National Science Foundation, under Grants No. PHY-0969510, the LHC Theory Initiative, No. PHY-1417317, and No. PHY-1619867. A. K. would like to thank the Theory Group at CERN, where part of this work was carried out, for its kind hospitality. T. S. acknowledges support in the form of a Westfälische Wilhelms-Universität Internationalization scholarship.

[1] G. Aad *et al.* (ATLAS Collaboration), Phys. Lett. B **740**, 222 (2015).
[2] G. Aad *et al.* (ATLAS Collaboration), Eur. Phys. J. C **75**, 349 (2015).
[3] V. Khachatryan *et al.* (CMS Collaboration), J. High Energy Phys. 09 (2014) 087; 10 (2014) 106.
[4] V. Khachatryan *et al.* (CMS Collaboration), Eur. Phys. J. C **75**, 251 (2015).
[5] G. Aad *et al.* (ATLAS Collaboration), Phys. Lett. B **749**, 519 (2015).
[6] D. de Florian *et al.* (LHC Higgs Cross Section Working Group), arXiv:1610.07922.
[7] ATLAS Collaboration, Report Nos. ATLAS-CONF-2016-058, ATLAS-CONF-2016-067, ATLAS-CONF-2016-068, ATLAS-CONF-2016-080.
[8] (CMS Collaboration), Report Nos. CMS-PAS-HIG-15-008, CMS-PAS-HIG-16-004, CMS-PAS-HIG-16-020, CMS-PAS-HIG-16-022, CMS-PAS-HIG-16-038, CMS-PAS-HIG-17-004.
[9] W. Beenakker, S. Dittmaier, M. Krämer, B. Plumper, M. Spira, and P. M. Zerwas, Phys. Rev. Lett. **87**, 201805 (2001); Nucl. Phys. **B653**, 151 (2003).
[10] L. Reina and S. Dawson, Phys. Rev. Lett. **87**, 201804 (2001); L. Reina, S. Dawson, and D. Wackeroth, Phys. Rev. D **65**, 053017 (2002); S. Dawson, L. H. Orr, L. Reina, and D. Wackeroth, Phys. Rev. D **67**, 071503 (2003); S. Dawson, C. Jackson, L. H. Orr, L. Reina, and D. Wackeroth, Phys. Rev. D **68**, 034022 (2003).
[11] V. Hirschi, R. Frederix, S. Frixione, M. V. Garzelli, F. Maltoni, and R. Pittau, J. High Energy Phys. 05 (2011) 044.
[12] R. Frederix, S. Frixione, V. Hirschi, F. Maltoni, R. Pittau, and P. Torrielli, Phys. Lett. B **701**, 427 (2011).
[13] M. V. Garzelli, A. Kardos, C. G. Papadopoulos, and Z. Trocsanyi, Europhys. Lett. **96**, 11001 (2011).
[14] H. B. Hartanto, B. Jager, L. Reina, and D. Wackeroth, Phys. Rev. D **91**, 094003 (2015).
[15] S. Frixione, V. Hirschi, D. Pagani, H. S. Shao, and M. Zaro, J. High Energy Phys. 09 (2014) 065.
[16] S. Frixione, V. Hirschi, D. Pagani, H.-S. Shao, and M. Zaro, J. High Energy Phys. 06 (2015) 184.
[17] Y. Zhang, W. G. Ma, R. Y. Zhang, C. Chen, and L. Guo, Phys. Lett. B **738**, 1 (2014).
[18] A. Denner and R. Feger, J. High Energy Phys. 11 (2015) 209.
[19] A. Denner, J. N. Lang, M. Pellen, and S. Uccirati, J. High Energy Phys. 02 (2017) 053.
[20] S. Dittmaier *et al.* (LHC Higgs Cross Section Working Group Collaboration), arXiv:1101.0593.
[21] R. Bonciani, S. Catani, M. L. Mangano, and P. Nason, Phys. Lett. B **575**, 268 (2003).
[22] S. M. Aybat, L. J. Dixon, and G. F. Sterman, Phys. Rev. Lett. **97**, 072001 (2006); Phys. Rev. D **74**, 074004 (2006).
[23] A. Kulesza, L. Motyka, T. Stebel, and V. Theeuwes, J. High Energy Phys. 03 (2016) 065.
[24] A. Kulesza, L. Motyka, T. Stebel, and V. Theeuwes, *Proc. Sci.*, LHCP2016 (2016) 084.
[25] H. T. Li, C. S. Li, and S. A. Li, Phys. Rev. D **90**, 094009 (2014).
[26] A. Broggio, A. Ferroglia, B. D. Pecjak, A. Signer, and L. L. Yang, J. High Energy Phys. 03 (2016) 124.
[27] A. Broggio, A. Ferroglia, G. Ossola, and B. D. Pecjak, J. High Energy Phys. 09 (**2016**) 089.
[28] A. Broggio, A. Ferroglia, B. D. Pecjak, and L. L. Yang, J. High Energy Phys. 02 (**2017**) 126.
[29] A. Broggio, A. Ferroglia, G. Ossola, B. D. Pecjak, and R. D. Sameshima, J. High Energy Phys. 04 (2017) 105.
[30] G. Sterman and M. Zeng, J. High Energy Phys. 05 (2014) 132.
[31] N. Kidonakis, G. Oderda, and G. Sterman, Nucl. Phys. **B531**, 365 (1998).
[32] H. Contopanagos, E. Laenen, and G. F. Sterman, Nucl. Phys. **B484**, 303 (1997).
[33] M. Czakon, A. Mitov, and G. F. Sterman, Phys. Rev. D **80**, 074017 (2009).
[34] N. Kidonakis and G. Sterman, Nucl. Phys. **B505**, 321 (1997).
[35] L. J. Dixon, L. Magnea, and G. F. Sterman, J. High Energy Phys. 08 (2008) 022.
[36] N. Kidonakis, G. Oderda, and G. Sterman, Nucl. Phys. **B525**, 299 (1998).
[37] A. Ferroglia, M. Neubert, B. D. Pecjakm, and L. L. Yang, Phys. Rev. Lett. **103**, 201601 (2009).
[38] A. Ferroglia, M. Neubert, B. D. Pecjak, and L. L. Yang, J. High Energy Phys. 11 (**2009**) 062.
[39] S. Catani, M. L. Mangano, P. Nason, and L. Trentadue, Nucl. Phys. **B478**, 273 (1996).
[40] S. Catani, D. de Florian, M. Grazzini, and P. Nason, J. High Energy Phys. 07 (2003) 028.
[41] A. J. Buras, Rev. Mod. Phys. **52**, 199 (1980).
[42] V. Ahrens, A. Ferroglia, M. Neubert, B. D. Pecjak, and L. L. Yang, J. High Energy Phys. 09 (2010) 097.
[43] S. Catani, S. Dittmaier, M. H. Seymour, and Z. Trocsanyi, Nucl. Phys. **B627**, 189 (2002).
[44] W. Beenakker, S. Brensing, M. Kramer, A. Kulesza, E. Laenen, and I. Niessen, J. High Energy Phys. 01 (2012) 076.
[45] W. Beenakker, T. Janssen, S. Lepoeter, M. Krämer, A. Kulesza, E. Laenen, I. Niessen, S. Thewes, and T. Van Daal, J. High Energy Phys. 10 (2013) 120.
[46] R. Bonciani, S. Catani, M. L. Mangano, and P. Nason, Nucl. Phys. **B529**, 424 (1998).
[47] E. L. Berger and H. Contopanagos, Phys. Rev. D **57**, 253 (1998).
[48] N. Kidonakis, Phys. Rev. D **64**, 014009 (2001).
[49] N. Kidonakis, arXiv:1311.0283.
[50] J. Alwall, R. Frederix, S. Frixione, V. Hirschi, F. Maltoni, O. Mattelaer, H.-S. Shao, T. Stelzer, P. Torrielli, and M. Zaro, J. High Energy Phys. 07 (**2014**) 079.
[51] J. Butterworth *et al.*, J. Phys. G **43**, 023001 (2016).
[52] S. Dulat, T.-J. Hou, J. Gao, M. Guzzi, J. Huston, P. Nadolsky, J. Pumplin, C. Schmidt, D. Stump, and C.-P. Yuan, Phys. Rev. D **93**, 033006 (2016).
[53] L. A. Harland-Lang, A. D. Martin, P. Motylinski, and R. S. Thorne, Eur. Phys. J. C **75**, 204 (2015).
[54] R. D. Ball *et al.* (NNPDF Collaboration), J. High Energy Phys. 04 (2015) 040.
[55] J. Gao and P. Nadolsky, J. High Energy Phys. 07 (2014) 035.
[56] S. Carrazza, S. Forte, Z. Kassabov, J. I. Latorre, and J. Rojo, Eur. Phys. J. C **75**, 369 (2015).